

Article

Upscaling Gross Primary Production from Leaf to Canopy for Potato Crop (*Solanum tuberosum* L.)

Fabio Ernesto Martínez-Maldonado ¹, Angela María Castaño-Marín ¹, Gerardo Antonio Góez-Vinasco ²
and Fabio Ricardo Marin ^{3,*}

¹ Corporación Colombiana de Investigación Agropecuaria—AGROSAVIA, Bogotá 250047, Colombia

² Grupo de Investigación de Agua y Saneamiento, Universidad Tecnológica de Pereira—UTP, Pereira 660003, Colombia

³ Luiz de Queiroz, College of Agriculture, University of São Paulo, Piracicaba 13418-900, SP, Brazil

* Correspondence: fabio.marin@usp.br

Abstract: Estimating gross primary production (GPP) is important to understand the land–atmosphere CO₂ exchange for major agroecosystems. Eddy covariance (EC) measurements provide accurate and reliable information about GPP, but flux measurements are often not available. Upscaling strategies gain importance as an alternative to the limitations of the use of the EC. Although the potato provides an important agroecosystem for worldwide carbon balance, there are currently no studies on potato GPP upscaling processes. This study reports two GPP scaling-up approaches from the detailed leaf-level characterization of gas exchange of potatoes. Multilayer and big leaf approaches were applied for extrapolating chamber and biometric measurements from leaf to canopy. Measurements of leaf area index and photosynthesis were performed from planting to the end of the canopy life cycle using an LP-80 ceptometer and an IRGA Li-Cor 6800, respectively. The results were compared to concurrent measurements of surface–atmosphere GPP from the EC measurements. Big-leaf models were able to simulate the general trend of GPP during the growth cycle, but they overestimated the GPP during the maximum LAI phase. Multilayer models correctly reproduced the behavior of potato GPP and closely predicted both: the daily magnitude and half-hourly variation in GPP when compared to EC measurements. Upscaling is a reliable alternative, but a good treatment of LAI and the photosynthetic light-response curves are decisive factors to achieve better GPP estimates. The results improved the knowledge of the biophysical control in the carbon fluxes of the potato crop.

Keywords: carbon flux; gross primary productivity; upscaling; eddy covariance method



Citation: Martínez-Maldonado, F.E.; Castaño-Marín, A.M.; Góez-Vinasco, G.A.; Marin, F.R. Upscaling Gross Primary Production from Leaf to Canopy for Potato Crop (*Solanum tuberosum* L.). *Climate* **2022**, *10*, 127. <https://doi.org/10.3390/cli10090127>

Received: 22 July 2022

Accepted: 24 August 2022

Published: 29 August 2022

Publisher's Note: MDPI stays neutral with regard to jurisdictional claims in published maps and institutional affiliations.



Copyright: © 2022 by the authors. Licensee MDPI, Basel, Switzerland. This article is an open access article distributed under the terms and conditions of the Creative Commons Attribution (CC BY) license (<https://creativecommons.org/licenses/by/4.0/>).

1. Introduction

Gross primary production (GPP) is a key ecosystem process that decreases the atmospheric carbon dioxide (CO₂) concentration [1–3]. CO₂ flux information [1] is necessary to improve the knowledge of the potential of ecosystems to grow and mitigate climate change [4,5]. Although eddy covariance (EC) measurements provide accurate and reliable information about carbon and energy balances at the ecosystem level, flux measurements are often not available in many places [6]. Therefore, different methodologies are needed to estimate GPP based on extrapolations of chamber and biometric measurements and the canopy upscaling process using readily measurable meteorological and environmental variables [4,7,8].

Upscaling the GPP from leaf to canopy is challenging because of the large micro-environment [light, temperature, vapor pressure deficit (VPD)] variability within plant canopies at both the vertical and horizontal dimensions [9,10]. A common strategy to represent carbon uptake during gross primary production (GPP) is through photosynthetic light use efficiency models based on photosynthetic light-response curves and light distribution through the canopy [1,11–16], assuming that light is the primary driver of vertical variation

in photosynthesis [17]. Nevertheless, canopy estimates require additional features such as light distribution through the canopy, canopy structure (mean leaf angle and leaf area index), and vertical profiles of weather variables within and above the crop [9,18].

Scaling methods vary with different complexity from the simplest one-big leaf [19–23], to two-big leaf models [22,24,25] and multilayer models [10,26–29]. The big leaf model is a representation of a canopy as a single giant leaf [18], which can be parameterized under a tractable mathematical solution at the canopy level [16]. In most plant species, the photosynthetic system is bulked in the upper layer of the canopy, and light decreases faster in horizontal canopies than in vertical ones [14]. Since the leaves in the potato canopy have a horizontal tendency [30,31], an approach that treats vegetation as a big leaf where the canopy GPP predictions are proportional to the photosynthesis of topmost unshaded leaves [16] could be useful. However, since the canopy is arbitrarily represented by a single leaf, it treats sunlit and shaded leaves within the canopy equally. In other words, the model assumes that there is no uncertainty introduced by ignoring the shaded fraction of the canopy, which results in an overestimation of flux rates [16,22,24,25].

In the multilayer model, the canopy is divided into n layers and light intensity declines with depth into the canopy as a function of the leaf area index [18,32]. Consequently, canopy photosynthesis is calculated separately for each layer. In general, multilayer models consider variations in the light level within the canopy, leaf inclination, and other leaf aspects as well as the variation of air temperature, wind speed, humidity, and CO₂ concentration [13,18,22]. The model calculates the net photosynthetic rate (A_n) for each layer, using the absorptance and the respective layer's leaf area [1,18,22,33].

Several researchers have attempted to evaluate the performance of different upscaling schemes with flux measurements (for wheat, shrublands, broadleaf, Amazonian, and conifer forests) [1,34–36], and have shown that the big-leaf approach matches overestimate or underestimate EC measurements [13,15,36]. Other studies have demonstrated the improved accuracy of multilayer models for GPP calculations [13,15,36]. Potatoes are critical for the food security of people across South America, Africa, and Asia, feeding more than one billion people worldwide [37,38]. It is the 4th most important crop in terms of global production [39], since more than 19 million hectares are cultivated around the world, making potatoes an important agroecosystem for worldwide carbon and greenhouse gas (GHG) balances [39–41]. However, despite the importance of potatoes, there are currently no studies on potato GPP upscaling processes as an alternative to the limitations inherent to EC techniques to obtain GPP contributions to the net ecosystem exchange.

This study aimed to test big-leaf and multilayer upscaling strategies for potato canopy GPP estimation. Our scaling proposal is based on the light profile within the canopy and photosynthetic light-response curves (A_n – I curves). The analytical solution uses models of photosynthesis such as the nonrectangular hyperbola and exponential model to describe light-driven photosynthesis in conjunction with Beer's law for the canopy light profile. The scaled-up estimates of canopy GPP were compared to concurrent measurements of surface–atmosphere GPP from the EC technique. To our knowledge, this study is the first to investigate upscaling strategies for potato canopy GPP estimation using EC data. This upscaling proposal might provide a useful and validated alternative to the EC technique and could be extrapolated to other potato cultivars to obtain canopy GPP estimations from infra-red gas analyzer (IRGA) measurements.

Specifically, the study reports the performance of two GPP scaling-up modeling approaches from the detailed leaf-level characterization of the gas exchange of potatoes. We addressed the following specific questions in our study: (1) what are the differences in the upscaled GPP between the two approximations? (2) why do these differences occur? (3) which model is the closest to the GPP obtained from the EC data?

2. Materials and Methods

2.1. Site Description

This study was conducted in the Colombian Andean Region, Western Savanna Province of the department of Cundinamarca. The potato (*Solanum tuberosum* L. Diacol Capiro Cultivar) cropping system was planted in a 3.11 hectare (ha) commercial plot, under a fixed-sprinkler irrigation system, located in the municipality of Subachoque (4.888668 N, −74.18668 W; ~2609 m asl). The crop was sown on 22 January 2021, with a plant density of 33333 pl ha^{−1}. The site was located over a fluvio-lacustrine plain with a flat landscape, with an average annual temperature ranging from 12 to 14 °C and an annual precipitation from 800 to 1000 mm with a bimodal distribution. The June–August and December–February periods have the lowest rainfall [8] due to the double passage of the Intertropical Convergence Zone (ITCZ). The soils are deep and well drained with the presence of volcanic ash and correspond to the Andisol order [42].

2.2. Microclimate and Eddy Covariance (EC) Measurements

Net carbon exchange and microclimatic variables were continuously recorded using the EC technique. The equipment was installed on 3 February 2021 (12 days post planting, DPP), and the measurements were taken until the end of the canopy life cycle on 9 June 2021 (138 DPP). The EC tower included an IRGASON with an open-path gas analyzer (EC 150, Campbell Scientific, Inc., Logan, UT, USA) and a 3D sonic anemometer (CSAT3A, Campbell Scientific, Inc., Logan, UT, USA). Both are operated by a separate electronic module (EC100, Campbell Scientific, Inc., Logan, UT, USA). The EC tower and additional sensor configuration are described by [8].

2.3. NEE Partitioning

The non-linear Mitscherlich light-response function, which parametrizes the net ecosystem exchange (NEE) against the photosynthetic photon flux density (PPFD), was used to partition diurnal NEE (solar global radiation > 1 W m^{−2}) into ecosystem respiration (R_{eco}) and GPP [43,44] as follows:

$$NEE = -(A_{gmax} + R_d) * \left(1 - \exp\left(\frac{-\Phi * I_{inc}}{A_{gmax} + R_d}\right)\right) + R_d \quad (1)$$

where A_{gmax} is the CO₂ uptake at light saturation [$\mu\text{mol}(\text{CO}_2) \text{m}^{-2} \text{s}^{-1}$]; R_d is the respiration term [$\mu\text{mol}(\text{CO}_2) \text{m}^{-2} \text{s}^{-1}$]; and Φ is the quantum yield efficiency [$\mu\text{mol}(\text{CO}_2) \mu\text{mol}(\text{photon})^{-1}$], i.e., the initial slope of the photosynthetic light-response curve, and I_{inc} is the incident PPFD [$\mu\text{mol}(\text{photon}) \text{m}^{-2} \text{s}^{-1}$].

For each day, a set of parameters was calculated through non-linear regression, using a subset of NEE and PPFD data within a centered moving window of 14 days. For each diurnal half-hour of the same day, GPP was estimated by subtracting R_d from the non-linear Mitscherlich light-response function. R_{eco} was calculated by subtracting the modeled GPP from the measured NEE. Data postprocessing, quality control, gap-filling, energy balance closure, uncertainty, and statistical analysis methods were applied, following the procedures described in [8].

2.4. Leaf-Level Measurements

At the leaf scale, we used an infrared gas analyzer IRGA LICOR 6800 IRGA system (LI-COR Biosciences, Lincoln, Nebraska, USA) to measure (1) the net photosynthetic rate at leaf scale (A_n) [$\mu\text{mol}(\text{CO}_2) \text{m}^{-2} \text{s}^{-1}$] as a function of PPFD, ranging from 50 to 2000 $\mu\text{mol}(\text{photon}) \text{m}^{-2} \text{s}^{-1}$ (A_n -I curves); and (2) A_n -I curves were recorded in three strata of the plant canopy: the upper stratum (topmost unshaded leaves), the middle stratum, and the low stratum (bottommost shaded leaves). Measurements were taken at 28, 36, 41, 52, 66, 71, 77, 91, 105, 117, and 130 days post planting (DPP) between 9:00 and 11:00 am in three plants. On the same days, the accumulated leaf area index (LAI) was also determined for each layer

of the plant canopy in 15 randomly selected plants using an ACCUPAR LP-80 ceptometer (METER Group, Inc., Pullman, WA, USA) with an external Apogee SQ110 PPF sensor from 0 to 4000 $\mu\text{mol (photon) m}^{-2} \text{s}^{-1}$ and 80 probe PPF sensors at the measurement bar. LAI data for the three canopy layers (upper, middle, and low) were fitted to third-degree and fourth-degree polynomial regressions.

Leaf insertion angles were determined using a compass and protractor, marking the leaf inclination angle. Subsequently, an analysis of the distribution of foliar angles was carried out according to [30,45] to determine the mean density angle (MDA) and the value of the ratio of the horizontal to vertical axis of the ellipsoid or parameter x using the following equation:

$$x = 1.7433025 + \left(\frac{162.22048}{MDA} \right) \quad (2)$$

The extinction coefficient (K) between 8:00 and 17:30 h was estimated from the ellipsoidal equation [30] that relates the variation of K with the vertical and horizontal projections of the canopy elements (parameter x) and the zenith angle ψ :

$$K = \frac{\sqrt{x^2 + \tan^2 \psi}}{x + 1.774 (x + 1.182)^{-0.733}} \quad (3)$$

2.4.1. Upscaling Approaches

The upscaled canopy GPP was based on light-use-efficiency models. The photosynthetic light-response curves (An–I curves) were fitted to three different and well described mathematical models like rectangular hyperbola-based models: (1) Michaelis–Menten as in Baly and Smith [46,47]; (2) hyperbolic tangent-based models [48]; and (3) exponential-based models [49]. The mathematical models that better fit the An–I curve data obtained in the field measurements were determined via sum of squared residuals (SSR) comparison [50]. Models with the lowest SSR were found in Baly [46], Smith [47] and Webb [49], and they have basically the following structure:

$$A_n = \frac{\Phi * I * A_{gmax}}{\Phi * I + A_{gmax}} - R_d \quad (4)$$

Michaelis–Menten function (Baly) [46]

$$A_n = \frac{\Phi * I * A_{gmax}}{\sqrt{\Phi_{(I_0)}^2 * I^2 + A_{gmax}^2}} - R_d \quad (5)$$

Michaelis–Menten type function (Smith) [47]

$$A_n = \left\{ A_{gmax} \left[1 - \exp \left(- \frac{\Phi * I}{A_{gmax}} \right) \right] \right\} - R_d \quad (6)$$

Exponential type function (Webb) [49], where A_n is the net photosynthetic rate [$\mu\text{mol (CO}_2\text{) m}^{-2} \text{s}^{-1}$]; A_{gmax} is the light-saturated gross photosynthetic rate [$\mu\text{mol (CO}_2\text{) m}^{-2} \text{s}^{-1}$]; R_d is the dark respiration rate [$\mu\text{mol (CO}_2\text{) m}^{-2} \text{s}^{-1}$]; I is the photosynthetic photon flux density PPF [$\mu\text{mol (photon) m}^{-2} \text{s}^{-1}$] and Φ is the quantum yield of assimilation [$\mu\text{mol (CO}_2\text{) } \mu\text{mol (photon)}^{-1}$]. The light-saturated gross photosynthetic rate (A_{gmax}) and quantum yield of assimilation (Φ) data obtained from the light-use-efficiency models and for each canopy stratum (upper, middle, and low) were fitted to third-degree and fourth-degree polynomial regressions to describe their behavior during canopy growth over time.

2.4.2. Modeling Schemes for Gross Primary Production of the Canopy (GPP_{can}) Big-Leaf Approach (BL)

The gross primary production of the canopy (GPP_{can}) was integrated over the canopy using a rectangular hyperbola base function (Michaelis–Menten type model), where light intensities within a canopy were calculated using a negative exponential function with a canopy light extinction coefficient (k) [9,32,51]. The total net carbon uptake integrated over the canopy is:

$$GPP_{can} = \frac{A_{gmax}}{K} \ln \frac{\Phi * K * I + A_{gmax}}{(\Phi * I * K * e^{-KLAI}) + A_{gmax}} \quad (7)$$

where GPP_{can} is the gross primary production of the canopy [$\mu_{mol} (CO_2) m^{-2} s^{-1}$]; A_{gmax} is the light-saturated gross photosynthetic rate [$\mu_{mol} (CO_2) m^{-2} s^{-1}$] of the topmost unshaded leaves; I is the photosynthetic photon flux density PPFD [$\mu_{mol} (photon) m^{-2} s^{-1}$]; K is the extinction coefficient; and Φ is the quantum yield of assimilation [$\mu_{mol}(CO_2) \mu_{mol} (photon)^{-1}$]. The values of the asymptotic estimate of the maximum gross photosynthetic rate (A_{gmax}) [$\mu_{mol} (CO_2) m^{-2} s^{-1}$] and the quantum yield Φ [$\mu_{mol} (CO_2) \mu_{mol} (photon)^{-1}$] were obtained from the fitted rectangular hyperbola-based models Baly [46] and Smith [47] (Figure 1).

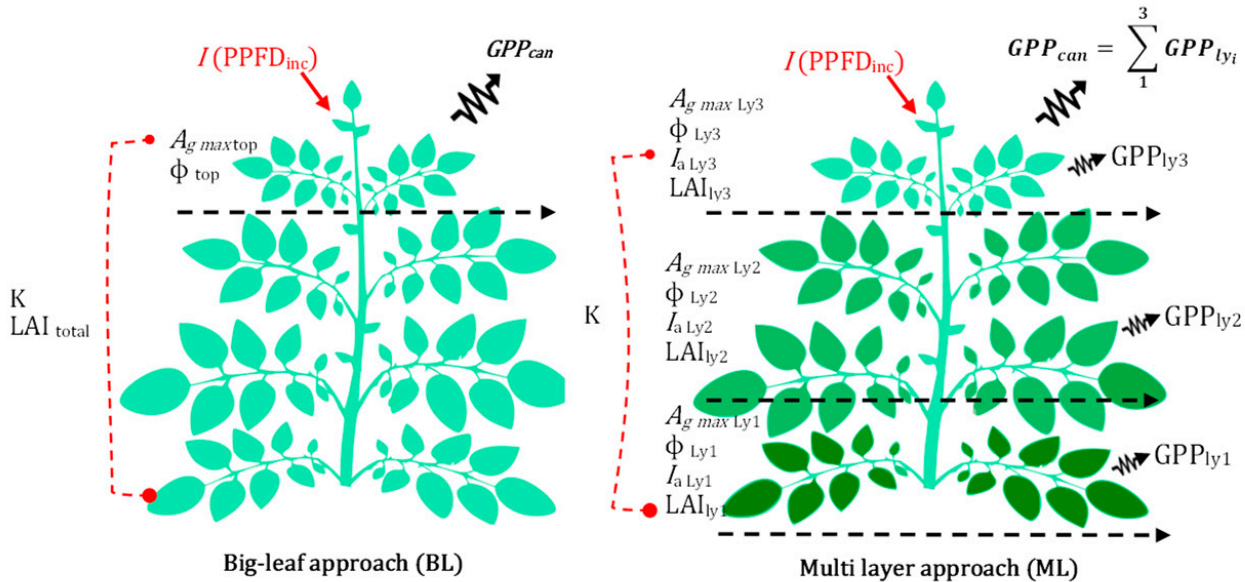


Figure 1. Schematic descriptions of the GPP_{can} upscaling models Big-leaf (BL) and Multilayer (ML).

Multilayer Approach (ML)

In this approach, the value of GPP_{can} was estimated from an extrapolation scheme based on Michaelis–Menten (rectangular hyperbola-based model) of Smith [51] and exponential Mitscherlich (Webb) [49] applied to three different layers of the canopy.

The canopy was divided in three layers, upper stratum (topmost unshaded leaves), middle stratum, and low stratum (bottommost shaded leaves), each one with defined LAI values. The leaf area index for each layer was obtained by the difference in leaf area index at the two heights bounding the layers. Thus, $LAI_i = LAI'_i - LAI'_{i-1}$, where LAI'_i is the LAI- ACCUPAR LP-80 measurement beneath the i_{th} layer. For n layers, $LAI'_n \equiv LAI$.

The leaf gross assimilation (G_i) was computed for each layer by introducing the description of the incident and absorbed PPFD in each layer in the Michaelis–Menten (Smith) [47] and Mitscherlich (Webb) [49] functions:

$$G_{i\ Smith} = \frac{\Phi_i * I_{ai} * A_{gmax_i}}{\sqrt{\Phi_i^2 * I_{ai}^2 + A_{gmax_i}^2}} \quad (8)$$

$$G_{i\text{ Webb}} = \left\{ A_{gmax_i} \left[1 - \exp \left(\frac{\Phi_i * I_{ai}}{A_{gmax_i}} \right) \right] \right\} \quad (9)$$

where G_i is leaf gross assimilation; A_{gmax} is light-saturated gross photosynthetic rate [$\mu\text{mol}(\text{CO}_2) \text{ m}^{-2} \text{ s}^{-1}$] for the layer i ; Φ is the quantum yield of assimilation for the layer i [$\mu\text{mol}(\text{CO}_2) \mu\text{mol}(\text{photon})^{-1}$]. A_{gmax} and Φ are parameters estimated from the mathematical models Michaelis–Menten (Smith) [47] and Mitscherlich (Webb) [49]. I_{ai} is the absorbed PPFD [$\mu\text{mol}(\text{photon}) \text{ m}^{-2} \text{ s}^{-1}$] for each layer, computed using Beer's law and the approach by Monsi et al. [14] and Sellers et al. [52]:

$$I_{ai} = I * (1 - e^{-K \text{ LAI}_i}) \quad (10)$$

where LAI_i is the leaf area index for each layer; I is the incident PPFD [$\mu\text{mol}(\text{photon}) \text{ m}^{-2} \text{ s}^{-1}$] above the canopy (measured every 30 min by the EC station) for the top layer, or the transmitted PPFD irradiance (I_{ti}) from cumulated leaf area index (LAI_c) of the layers above the layer i estimated by:

$$I_{ti} = I * e^{-K \text{ LAI}_c} \quad (11)$$

The gross primary production for each canopy layer (GPP_{ly}) was computed every 30 min by multiplying G_i by the canopy scaling factor, as shown in Equation (13) [32,51].

$$\text{GPP}_{ly_i} = G_i * \left\{ \frac{1 - e^{-K \text{ LAI}_i}}{K} \right\} \quad (12)$$

Then, the gross primary production of the entire canopy (GPP_{can}) was estimated by summing the contribution of each layer (Figure 1):

$$\text{GPP}_{can} = \sum_1^3 \text{GPP}_{ly_i} \quad (13)$$

2.4.3. Accuracy Assessment

The model's goodness of fit was evaluated using RMSE. Complementary accuracy assessment was made through the variation of regression data around the 1:1 line.

3. Results

3.1. Meteorological Conditions

The daily mean PPFD was $724.5 \pm 216.7 \mu\text{mol}(\text{photon}) \text{ m}^{-2} \text{ s}^{-1}$. The average daily mean temperature (T_{mean}) and the maximum air temperature (T_{max}) were $16.51 \text{ }^\circ\text{C} \pm 1.02$ and $19.73 \text{ }^\circ\text{C} \pm 1.23$, respectively. The average daily maximum vapor pressure deficit (VPD) was $0.73 \text{ kPa} \pm 0.25$ and the average irrigated daily mean VPD was $0.38 \text{ kPa} \pm 0.16$. The accumulated rainfall was 306 mm, uniformly distributed, but including the relatively drier period from 13 March to 22 April 2021 (50–90 DPP). The soil water content (SWC) was near to field capacity in almost all the crop growth cycles (Figure 2).

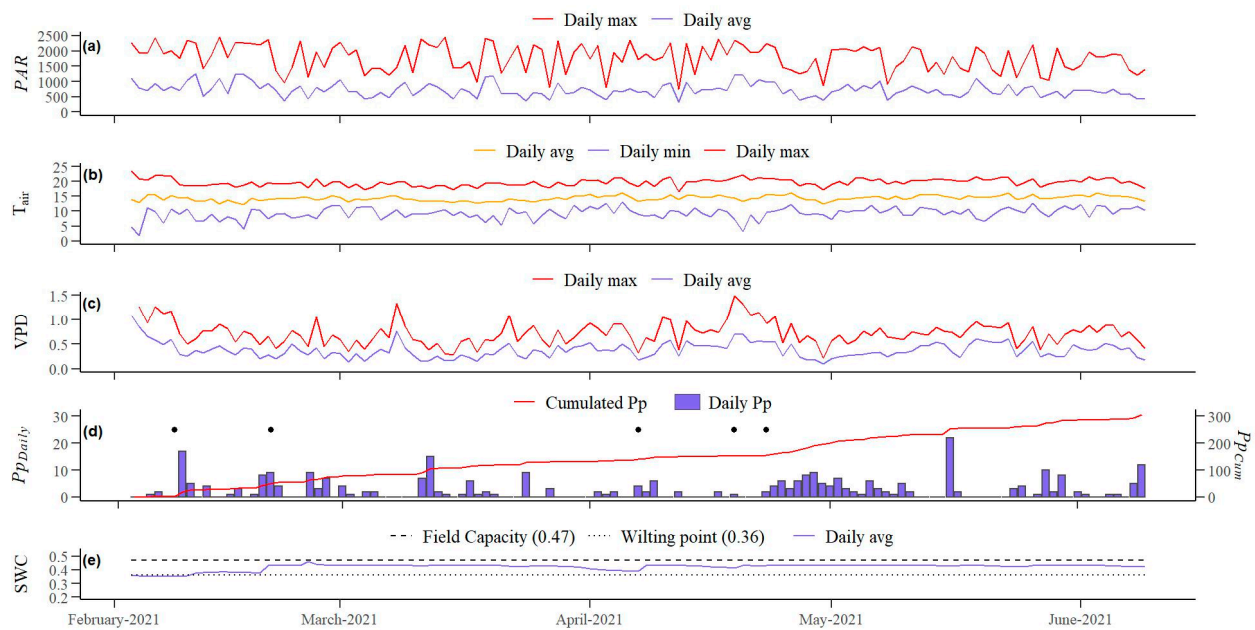


Figure 2. Meteorological variables observed along the experiment (from 3 February to 9 June 2021). (a) average and maximum daily photosynthetic active radiation (PPFD, $\mu\text{mol (photon) m}^{-2} \text{s}^{-1}$); (b) average, maximum, and minimum air temperature (T_{air} , $^{\circ}\text{C}$); (c) average and maximum daily vapor pressure deficit (VPD, kPa); (d) daily and cumulated precipitation (Pp, mm), shown as daily sum, black dots indicate irrigation times; (e) soil water content, (SWC, $\text{cm}^3 \text{cm}^{-3}$), measured at 0–20 cm depth, shown as daily mean values.

3.2. Leaf Area Index (LAI) Evolution

LAI is defined as the sum of the photosynthetically active leaf surfaces divided by the soil surface occupied by canopy and is the basic variable for relating the radiation intercepted by the canopy to the total incident radiation. The total LAI increased in an accelerated way, from the initial phase of crop growth to around 80 DPP, when the LAI peak reached 4.65. The accumulated LAI in the middle stratum had the same trend, increasing up to a maximum of 3.43 at 73 DPP. The LAI measured in the upper stratum remained around unity throughout the entire growth period of the crop (Figure 3).

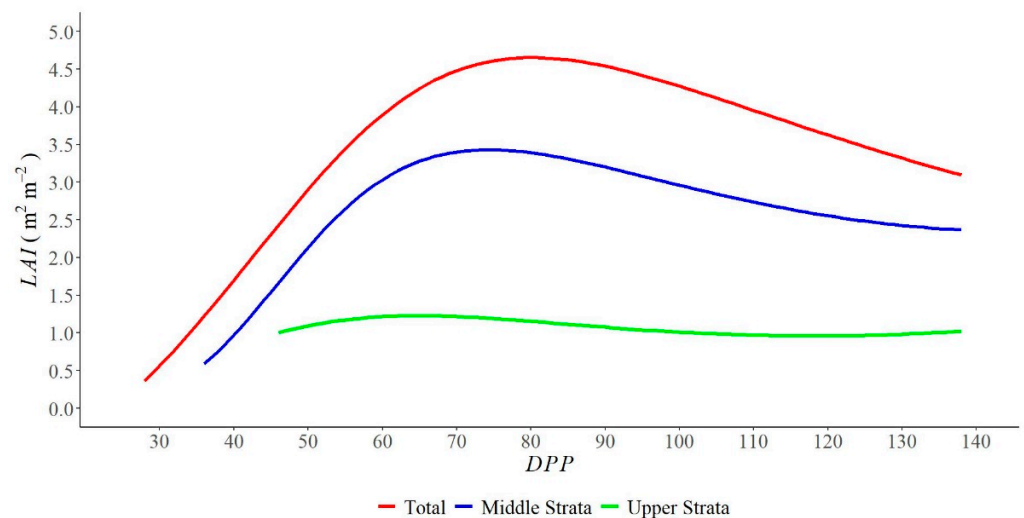


Figure 3. Accumulated leaf area index (LAI) through plant canopy, upper stratum (topmost unshaded leaves), middle stratum, and total of potatoes (*Solanum Tuberosum* L. Var. Diacol capiro) versus days post planting (DPP).

3.3. Photosynthetic Behavior through the Canopy

The response of the net assimilation rate to the incident photosynthetic photon flux density (PPFD) varied with canopy depth and leaf age. The leaves of the upper stratum presented the highest carbon assimilation (A_n) responses to PPFD. The largest A_n response to an incident PPFD was observed between 71 and 91 DPP. Maximum values around $23 \mu\text{mol} (\text{CO}_2) \text{m}^{-2} \text{s}^{-1}$ were obtained with PPFD higher than $900 \mu\text{mol} (\text{photon}) \text{m}^{-2} \text{s}^{-1}$ (Figure 4a). The middle leaves had a lower response of net photosynthetic rate (A_n) to photosynthetic photon flux density than the upper stratum leaves. The highest responses of A_n to PPFD were observed between 71 and 77 DPP. In this canopy position, A_n leaf values of around $20 \mu\text{mol} (\text{CO}_2) \text{m}^{-2} \text{s}^{-1}$ were obtained with a PPFD greater than $800 \mu\text{mol} (\text{photon}) \text{m}^{-2} \text{s}^{-1}$ (Figure 4b). The bottom leaves presented a limited (maximum average $9.7 \mu\text{mol} (\text{CO}_2) \text{m}^{-2} \text{s}^{-1}$) net photosynthetic rate response to PPFD in all evaluated dates. Although the highest response to PPFD was observed between 77 and 105 DPP, the highest possible assimilation values ($A_n < 15 \mu\text{mol} (\text{CO}_2) \text{m}^{-2} \text{s}^{-1}$) were obtained at low PPFD values ($500 \mu\text{mol} (\text{photon}) \text{m}^{-2} \text{s}^{-1}$) (Figure 4c). The declining tendency in net photosynthetic responses to PPFD was observed with leaf aging and canopy depth. The measured light response of A_n declined from the top (young and unshaded leaves) to the basal (old and most shaded leaves) within the potato canopy. Likewise, the net photosynthetic responses to PPFD were lower when canopy age was greater than 117 DPP in all canopy strata, revealing the impact of leaf age on potato leaf photosynthetic traits (Figure 4).

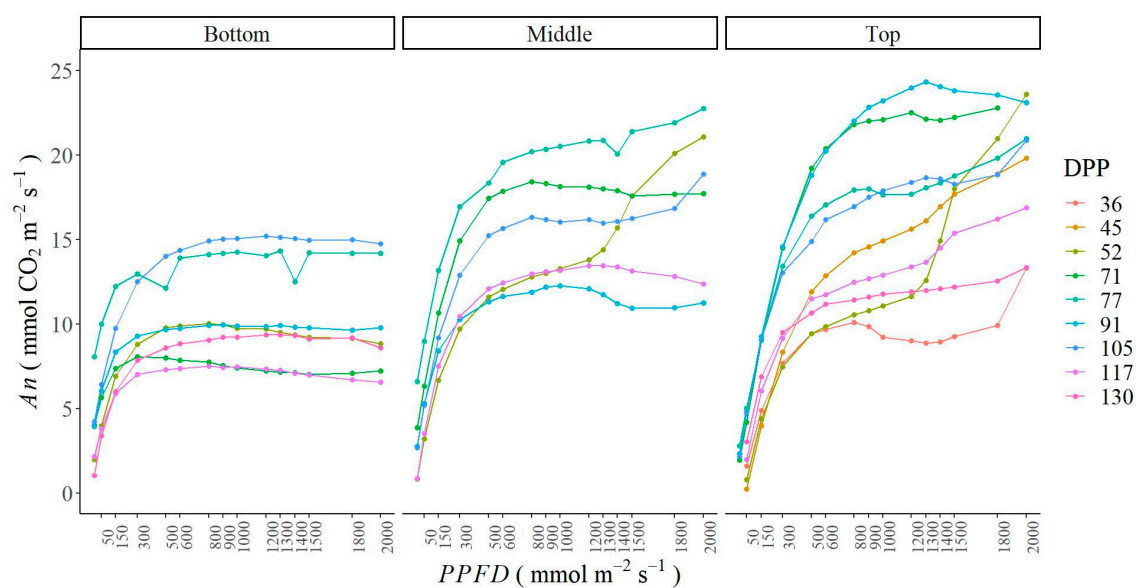


Figure 4. Measured response of net photosynthetic rate (A_n) for potato (*Solanum Tuberosum* L. Var. Diacol capiro) to photosynthetic photon flux density (PPFD) at different days post planting (DPP) on the bottommost shaded leaves (**left**), middle leaves (**center**), and the topmost unshaded leaves (**right**) of potatoes (*Solanum Tuberosum* L. Var. Diacol capiro).

The three models represented the variation of the photosynthetic traits with leaf aging and canopy depth well. The measured light-saturated net photosynthetic rate (A_{gmax}) and quantum yield of assimilation (Φ) reached their maximum at full canopy development, around the maximum LAI stage (60–90 DPP), and then declined gradually as leaves senesced (Figure 5). Regarding canopy leaf position, the three models showed an A_{gmax} declination from the top to the bottom of the canopy, where the lowest carbon assimilation rates at light saturation were observed. In contrast, by comparison with upper canopy leaves, values for Φ in the lower canopy were higher. The parameters A_{gmax} and Φ calculated throughout Michaelis–Menten (Smith) [47] and Mitscherlich (Webb) [49] models showed a similar trend and values for the three canopy strata. The values of A_{gmax} and Φ obtained from Michaelis–Menten (Baly) [46] were higher and varied over a wider range. In

addition, they presented variations in their behavior, easily observed in the leaves of the middle and lower canopy strata (Figure 5).

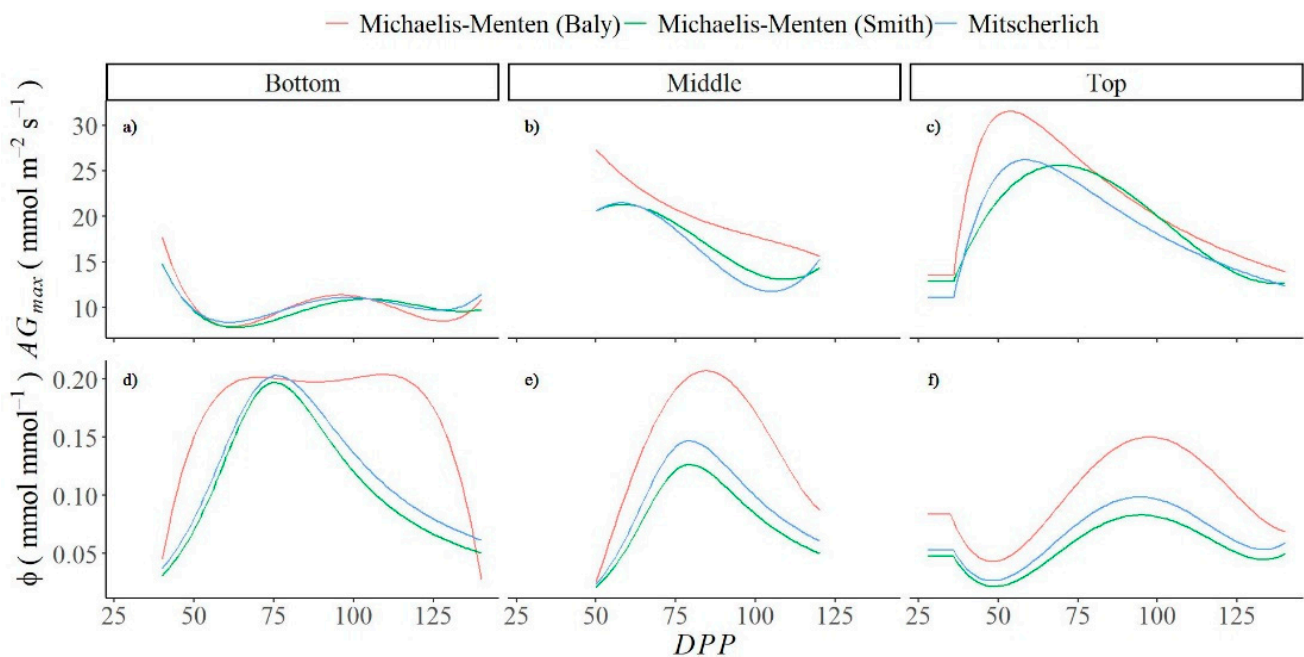


Figure 5. Parameters of light-saturated gross photosynthetic rate (A_{gmax}) and quantum yield of assimilation (Φ) for the topmost unshaded leaves ((c,f), respectively), middle stratum leaves((b,e), respectively), and the bottommost shaded leaves ((a,d), respectively) of potato (*Solanum Tuberosum* L. Var. Diacol capiro) calculated by the rectangular hyperbola Michaelis–Menten type function, Smith [47] and Baly [46], and by an exponential Mitscherlich function [49].

3.4. GPP Up Scaling

The measured EC GPP shows a progressive increase from 28 DPP until a maximum GPP ($500 \text{ kg C ha}^{-1} \text{ day}^{-1}$) occurred at 88 DPP. From 90 to 138 DPP, the daily GPP decreased progressively until a minimum value of $200 \text{ kg C ha}^{-1} \text{ day}^{-1}$. Multilayer (ML) models correctly reproduce the behavior of potato GPP over time as well as the magnitude of the maximum values that occur around 90 DPP. In the ML Michaelis–Menten (Smith) model [47], the GPP was underestimated between 36 and 66 DPP (measured GPP was up to 170% higher) and between 87 and 117 DPP (measured GPP was 50% higher). The multilayer model-based Mitscherlich (Webb) function [49] underestimates the GPP during most of the cycle. The greatest differences were in the period between 28 and 65 DPP and 95 to 117 DPP. The Big-leaf (BL) Michaelis–Menten (Smith) model [47] underestimates the GPP mainly between 28–70 DPP. After this period, however, GPP values were close to the measured GPP. The maximum GPP reached is 50% greater than the one measured with the EC tower. However, BL models overestimated GPP, mainly during the maximum LAI phase (80–90 DPP) (Figure 6).

The modeled and measured GPP showed variations of the half-hourly GPP mean throughout the day and across growth stages (Figure 7). In the tuberization stage, GPP measured rates increased progressively throughout the day, reaching a maximum of $1.30 \pm 0.19 \text{ mg CO}_2 \text{ m}^{-2} \text{ s}^{-1}$ between 9 to 13 h. In this stage, the ML Michaelis–Menten (Smith) model [47] predicted the measured values more closely than the other models. In the vegetative and tuber bulking stages, half-hourly GPP maximums ($0.83 \pm 0.37 \text{ mg CO}_2 \text{ m}^{-2} \text{ s}^{-1}$ and $0.96 \pm 0.18 \text{ mg CO}_2 \text{ m}^{-2} \text{ s}^{-1}$, respectively) were also found between 9 and 13 h. Again, the GPP predicted by the ML Michaelis–Menten (Smith) model [47] was closer to the measured values. The BL Michaelis–Menten (Baly) model [46] overestimates the half-hourly GPP in all stages (Figure 7).

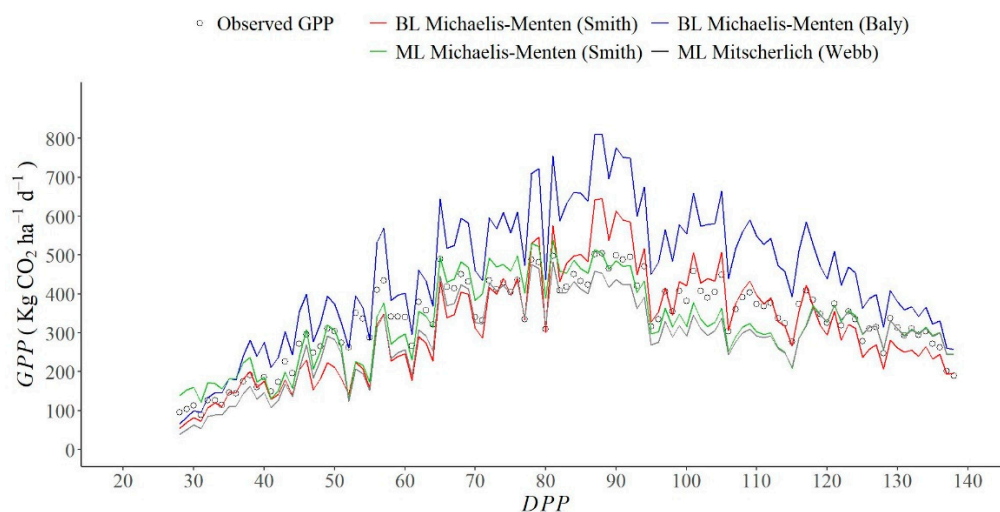


Figure 6. Daily gross primary production (GPP) estimated with the scaling up Big-Leaf—BL (red, blue solid lines) and Multilayer—ML (green, black solid lines) models and Eddy Covariance—EC measurements (open circles), Vs. days post planting (DPP).

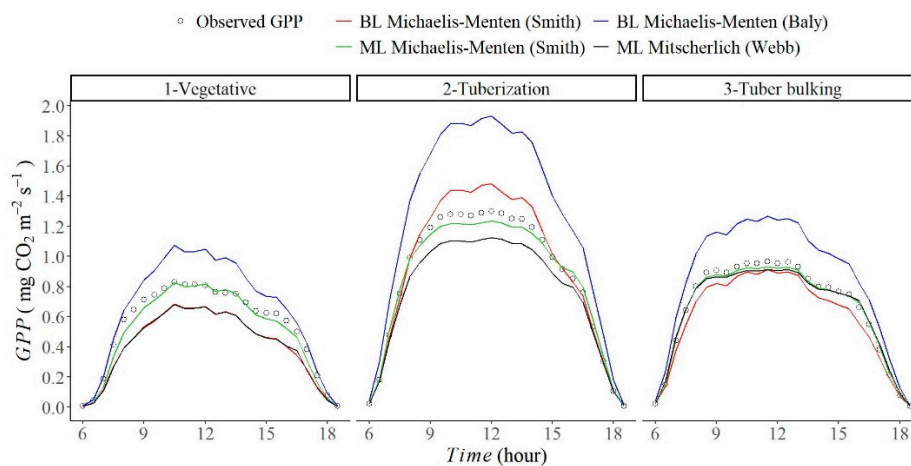


Figure 7. Half-hourly variation of gross primary production (GPP) estimated with the scaling up Big-leaf—BL (red and blue lines) and Multilayer—ML (green and yellow lines) models and with eddy covariance measurements (black line) in three different growth stages (vegetative, tuberization, tuber bulking) of potatoes (*Solanum Tuberosum* L. Var. Diacol capiro). Half-hourly averages are plotted.

Figure 8 shows day-to-day variations of GPP measured (obtained by the eddy covariance technique) versus the big-leaf and multilayer models. In general, the correlation coefficient r showed that the modeled and measured GPP values had a strong linear correlation. The RMSE value was higher for BL models than ML models, indicating a lower performance and hence less accuracy for BL models. Most of the ML GPP modeled vs. GPP measured data are closely distributed around the 1:1 line. This greater closeness of the multilayer models' scatter plot of the predicted value to the 1:1 line indicates a better accuracy than BL models (Figure 8a,b). The ML Michaelis–Menten (Smith) [47] based model had the highest accuracy due to its lowest RMSE (0.131) obtained, followed by the multilayer model based on the Mitscherlich (Webb) [49] function (RMSE = 0.155). Likewise, the daily variability in GPP is more accurately captured by the ML Michaelis–Menten (Smith) [47] model due to the linear regression showing the smallest deviation from the 1:1 line (Figure 8b).

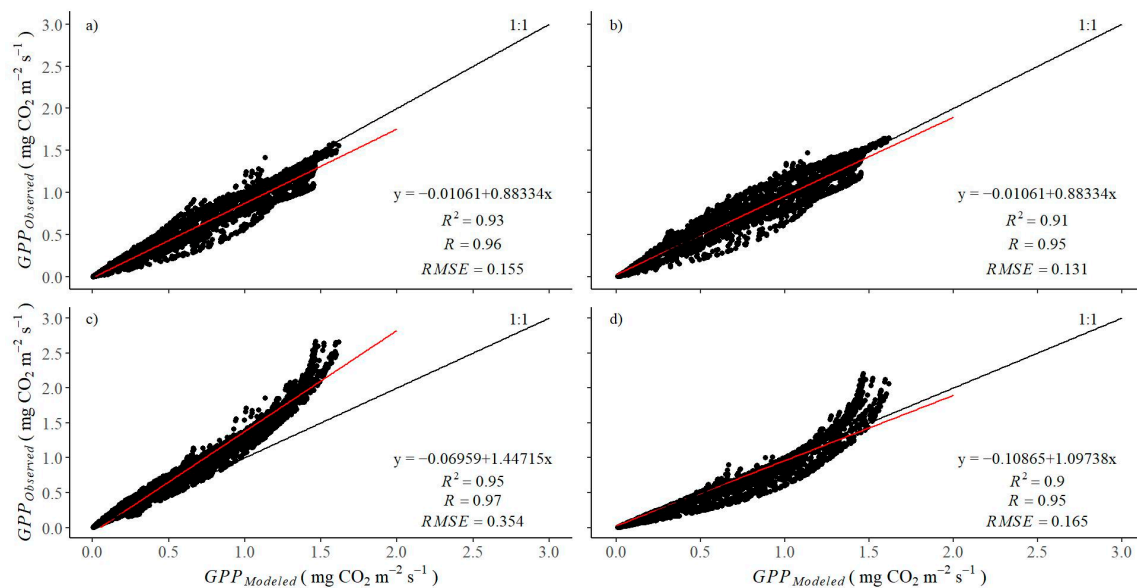


Figure 8. One-to-one comparison of the measured gross primary production (GPP) and the GPP simulated by (a) multilayer Mitscherlich (Webb), (b) multilayer Michaelis–Menten (Smith), (c) big-leaf Michaelis–Menten (Baly), and (d) big-leaf Michaelis–Menten (Smith) approaches. Equations, root mean squared error (RMSE), determination and correlation coefficients (R^2) are inserted inside graphs.

4. Discussion

The measured GPP has a close relationship with the carbon requirements of each crop growth stage. The maximum daily GPP and half-hourly GPP occur in the tuberization stage and maximum LAI (close to 90 DPP). The behavior of modeled data is consistent with our hypothesis: the big-leaf models overestimate the GPP, specifically during the period of maximum LAI and tuberization stage. Even though multilayer models tend to underestimate the GPP, they better described the daily GPP behavior, and their maximum values were close to the daily GPP and half-hourly GPP values determined by the EC station. Previous studies have shown that the big leaf approach overestimates EC measurements [24]. In particular, de Pury et al. [24] concludes that the performance of the big leaf model is strongly affected by the LAI and reports an overestimation of 50% in the GPP during the maximum LAI.

Big leaf assumes that the canopy has the same photosynthetic behavior. It has an inability to consider the variation in the CO_2 assimilation of the leaves along the canopy, especially the shaded leaves, which have differences in photosynthetic capacity. This model assumes that the entire canopy is a single unshaded leaf located at the canopy top (with an evident greater photosynthetic capacity) [36]. Therefore, the increase in the amount of foliage with these characteristics resulted in overestimations of the maximum LAI. In contrast, with the ML approach, the canopy is separated into layers with different light environments and photosynthetic capacities. In the maximum LAI, the topmost unshaded layer remains constant, and the remaining LAI is distributed between the intermediate and lower layers. Our results indicate that multilayer models performed better than big-leaf models at simulating GPP (as evidenced by ML RMSE being lower than BL RMSE). Some other researchers have also found better performance of ML models compared to BL models in maize and forests [1,34]. However, including several canopy layers for studying light interactions through the canopy requires more detailed input data. In our study for the big-leaf models, we used just 30 min data of PPF and the zenith angle, and the extinction coefficient was used to define the PPF attenuation through the canopy in a single LAI layer. In the multilayer models, in addition to daily data of the zenith angle and incident PPF, transmitted and absorbed radiation in each canopy layer were computed, as well as

the evolution of A_{gmax} , quantum yield of assimilation (Φ), and LAI in three different layers during growth was determined.

The main difference is the treatment of the LAI in each approach. In potatoes, Martinez-Maldonado et al. [8] demonstrated that the evolution of daily GPP is linked to the behavior of the LAI. Furthermore, a direct effect of changes in canopy architecture on simulated productivity has been shown [36]. This effect is not only linked to the number of photosynthetic leaves but also to the variability in the photosynthetic capacity throughout the canopy. Not all the leaves along the canopy behave like those of the upper stratum. There was a gradient in the photosynthetic capacity within the canopy depending on the age of the leaf, its position in the canopy, and its light environment. In this study, the photosynthetic behavior through the canopy showed that the leaf photosynthesis responses to PFD, the light-saturated net photosynthetic rate (A_{gmax}), and the quantum yield of assimilation (Φ) of the middle and bottom layers of the canopy were highly different from the upper unshaded leaves. Therefore, each stratum contributed in a different way to the total assimilation of the canopy and this contribution changes during the crop growth cycle.

The upscaling performance depends on the choice of the photosynthetic light-response curves (An–I curves). In the present study, the modeling of the GPP was achieved based on functions that describe and interpret the photosynthetic light responses of leaves. This interpretation works based on primary parameters such as light-saturated net photosynthetic rate (A_{gmax}) and quantum yield of assimilation (Φ). For C3 species, the theoretical quantum yield is around $0.1250 \mu\text{mol}(\text{CO}_2) \mu\text{mol}(\text{photon})^{-1}$ [50,53,54] and the maximum value of A_{gmax} ranges from 42 to $59 \mu\text{mol}(\text{CO}_2) \text{m}^{-2} \text{s}^{-1}$ [55]. Although, the functions used for upscaling had below typical C3 A_{gmax} values, the parameters deduced by the classical Michaelis–Menten (Baly) function were larger ($32 \mu\text{mol}(\text{CO}_2) \text{m}^{-2} \text{s}^{-1}$ and $0.15 \mu\text{mol}(\text{CO}_2) \mu\text{mol}(\text{photon})^{-1}$), in comparison to maximum values for Michaelis–Menten (Smith) ($25.6 \mu\text{mol}(\text{CO}_2) \text{m}^{-2} \text{s}^{-1}$ and $0.08 \mu\text{mol}(\text{CO}_2) \mu\text{mol}(\text{photon})^{-1}$) and for Webb ($26.2 \mu\text{mol}(\text{CO}_2) \text{m}^{-2} \text{s}^{-1}$ and $0.098 \mu\text{mol}(\text{CO}_2) \mu\text{mol}(\text{photon})^{-1}$). The above indicates that the Baly-based upscaling model overestimated the GPP due to its higher values in the photosynthetic capacity parameters. The Michaelis–Menten (Baly) function, which tends to overestimate the rate of photosynthesis at low and high irradiances, fails to reproduce the decline of photosynthesis at the photoinhibitory region [56–58] and overestimates A_{gmax} and quantum yield of assimilation (Φ), which has also been reported in Amazon forest species [59].

There are inherent limitations of An–I curves to capture the photosynthetic responses of the canopy, mainly for the upper leaves that were never fully light-saturated even under direct sunlight (Figure 2). However, the GPP calculated based on the parameters deduced from Michaelis–Menten (Smith) [47] and Mitscherlich (Webb) [49] in both big-leaf and multilayer approaches was closer to the measured GPP because they saturated at a lower PFD than the classical Michaelis–Menten (Baly) equation. In this regard, authors such as [13,60,61] indicate that the modeling of the GPP from the Mitscherlich exponential function led to more realistic saturation assimilation values. Among the several processes that need to be described in up scaling models, canopy light absorption is essential since it drives the energy available for photosynthesis. Especially in potatoes, the planophile leaves generate a pronounced light gradient with a possible large effect on total GPP that can be estimated using the analytical solution proposed in this work, which is based on light relations in the canopy using simplified models of photosynthesis.

5. Conclusions

The results improve the knowledge of biophysical control in carbon fluxes of potato crops and demonstrate the importance of both the characteristics of the canopy (LAI, leaf angle) and the light relationships of the plants in their immediate environment. Therefore, the photosynthetic light-response curve and a good treatment of the LAI are decisive factors in order to get closer GPP determinations. Big-leaf models are simpler and, although they can simulate the general trend of GPP during the growth cycle, they overestimate the GPP during

the maximum LAI since they assume that the canopy has the same photosynthetic behavior as the topmost unshaded leaves. The multilayer approaches allow us to understand not only the amount of leaf area available for photosynthesis but also how the photosynthetic capacity is redistributed in a canopy in relation to the age of the leaf, its position in the canopy, and the changing carbon demand during the crop cycle. Based on these results, the multilayer Michaelis–Menten (Smith) based model predicted more closely both the magnitude and the daily and half-hourly variation in GPP of eddy covariance measurements.

Finally, we demonstrated that models describing the net CO₂ assimilation by a plant leaf as a function of an increase in the photosynthetic photon flux density could be useful for potato GPP estimations. However, for future studies improving accuracy in the GPP upscaling requires descriptions that includes exponential profiles of leaf nitrogen and explore canopy chemistry models to scale leaf GPP to canopy.

Author Contributions: Conceptualization, F.E.M.-M.; methodology, F.E.M.-M., A.M.C.-M., G.A.G.-V. and F.R.M.; software, G.A.G.-V.; formal analysis, F.E.M.-M., A.M.C.-M. and G.A.G.-V.; investigation, F.E.M.-M., A.M.C.-M. and G.A.G.-V.; resources, A.M.C.-M.; data curation, F.E.M.-M. and G.A.G.-V.; writing—original draft, F.E.M.-M., A.M.C.-M., G.A.G.-V. and F.R.M.; writing—review and editing, F.R.M., F.E.M.-M., A.M.C.-M. and G.A.G.-V.; supervision, A.M.C.-M. and F.R.M.; project administration, A.M.C.-M.; funding acquisition, A.M.C.-M. All authors have read and agreed to the published version of the manuscript.

Funding: This research was funded by the Fondo de Ciencia, Tecnología e Innovación del Sistema General de Regalías, administered by the Fondo Nacional de Financiación para Ciencia, Tecnología e Innovación—Francisco José de Caldas, Programa Colombia BIO, Gobernación de Cundinamarca and Ministerio de Ciencia, Tecnología e Innovación (MINCIENCIAS) funding number 66153, and Corporación Colombiana de Investigación Agropecuaria (AGROSAVIA) funding number TV19 1000911.

Institutional Review Board Statement: Not applicable.

Informed Consent Statement: Not applicable.

Data Availability Statement: The datasets generated during and/or analyzed during the current study are available from the corresponding author on reasonable request.

Acknowledgments: This work is part of a larger project in Corporación Colombiana de Investigación Agropecuaria (AGROSAVIA) named Sistema de Información Agroclimática del cultivo de la papa en la región de Cundinamarca, Colombia (SIAP). We thank Zahara Lucia Lasso Paredes, Jose Alfredo Molina Varón, Pablo Edgar Jiménez, Óscar Dubán Ocampo Páez, and Jhon Alexander Martínez Morales, for their contribution in the equipment installation process, Julio Duarte for the language revision, and farmers Santiago Forero, Wilson Forero and Alejandro Forero for providing a suitable lot for the study.

Conflicts of Interest: The authors declare no conflict of interest.

References

1. Arkebauer, T.J.; Walter-Shea, E.A.; Mesarch, M.A.; Suyker, A.E.; Verma, S.B. Scaling up of CO₂ fluxes from leaf to canopy in maize-based agroecosystems. *Agric. For. Meteorol.* **2009**, *149*, 2110–2119. [[CrossRef](#)]
2. Suyker, A.E.; Verma, S.B.; Burba, G.G.; Arkebauer, T.J. Gross primary production and ecosystem respiration of irrigated maize and irrigated soybean during a growing season. *Agric. For. Meteorol.* **2005**, *131*, 180–190. [[CrossRef](#)]
3. Teubner, I.E.; Forkel, M.; Camps-Valls, G.; Jung, M.; Miralles, D.G.; Tramontana, G.; van der Schalie, R.; Vreugdenhil, M.; Möisinger, L.; Dorigo, W.A. A carbon sink-driven approach to estimate gross primary production from microwave satellite observations. *Remote Sens. Environ.* **2019**, *229*, 100–113. [[CrossRef](#)]
4. Wagle, P.; Xiao, X.; Suyker, A.E. Estimation and analysis of gross primary production of soybean under various management practices and drought conditions. *ISPRS J. Photogramm. Remote Sens.* **2015**, *99*, 70–83. [[CrossRef](#)]
5. Wagle, P.; Gowda, P.H.; Anapalli, S.S.; Reddy, K.N.; Northup, B.K. Growing season variability in carbon dioxide exchange of irrigated and rainfed soybean in the southern United States. *Sci. Total Environ.* **2017**, *593–594*, 263–273. [[CrossRef](#)]
6. Jiang, X.; Kang, S.; Tong, L.; Li, F.; Li, D.; Ding, R.; Qiu, R. Crop coefficient and evapotranspiration of grain maize modified by planting density in an arid region of northwest China. *Agric. Water Manag.* **2014**, *142*, 135–143. [[CrossRef](#)]

7. Malhi, Y.; Aragão, L.E.O.C.; Metcalfe, D.B.; Paiva, R.; Quesada, C.A.; Almeida, S.; Anderson, L.; Brando, P.; Chambers, J.Q.; da Costa, A.C.L.; et al. Comprehensive assessment of carbon productivity, allocation and storage in three Amazonian forests. *Glob. Chang. Biol.* **2009**, *15*, 1255–1274. [[CrossRef](#)]
8. Martínez-Maldonado, F.E.; Castaño-Marin, A.M.; Góez-Vinasco, G.A.; Marin, F.R. Gross Primary Production of Rainfed and Irrigated Potato (*Solanum tuberosum* L.) in the Colombian Andean Region Using Eddy Covariance Technique. *Water* **2021**, *13*, 3223. [[CrossRef](#)]
9. Eamus, D.; Huete, A.; Yu, Q. Modelling Leaf and Canopy Photosynthesis. *Veg. Dyn.* **2016**, 260–280.
10. Ran, L.; Pleim, J.; Song, C.; Band, L.; Walker, J.T.; Binkowski, F.S. A photosynthesis-based two-leaf canopy stomatal conductance model for meteorology and air quality modeling with WRF/CMAQ PX LSM. *J. Geophys. Res.* **2017**, *122*, 1930–1952. [[CrossRef](#)]
11. Waldo, S.; Chi, J.; Pressley, S.N.; O’Keeffe, P.; Pan, W.L.; Brooks, E.S.; Huggins, D.R.; Stöckle, C.O.; Lamb, B.K. Assessing carbon dynamics at high and low rainfall agricultural sites in the inland Pacific Northwest US using the eddy covariance method. *Agric. For. Meteorol.* **2016**, *218–219*, 25–36. [[CrossRef](#)]
12. Goudriaan, J. A simple and fast numerical method for the computation of daily totals of crop photosynthesis. *Agric. For. Meteorol.* **1986**, *38*, 249–254. [[CrossRef](#)]
13. Hoyaux, J.; Moureaux, C.; Tourneur, D.; Bodson, B.; Aubinet, M. Extrapolating gross primary productivity from leaf to canopy scale in a winter wheat crop. *Agric. For. Meteorol.* **2008**, *148*, 668–679. [[CrossRef](#)]
14. Monsi, M.; Saeki, T.; Schortemeyer, M. On the factor light in plant communities and its importance for matter production. *Ann. Bot.* **2005**, *95*, 549–567. [[CrossRef](#)] [[PubMed](#)]
15. Moureaux, C.; Debacq, A.; Hoyaux, J.; Suleau, M.; Tourneur, D.; Vancutsem, F.; Bodson, B.; Aubinet, M. Carbon balance assessment of a Belgian winter wheat crop (*Triticum aestivum* L.). *Glob. Chang. Biol.* **2008**, *14*, 1353–1366. [[CrossRef](#)]
16. Raulier, F.; Bernier, P.Y.; Ung, C.H. Canopy photosynthesis of sugar maple (*Acer saccharum*): Comparing big-leaf and multilayer extrapolations of leaf-level measurements. *Tree Physiol.* **1999**, *19*, 407–420. [[CrossRef](#)]
17. Bonan, G.B.; Patton, E.G.; Finnigan, J.J.; Baldocchi, D.D.; Harman, I.N. Moving beyond the incorrect but useful paradigm: Reevaluating big-leaf and multilayer plant canopies to model biosphere-atmosphere fluxes – a review. *Agric. For. Meteorol.* **2021**, *306*, 108435. [[CrossRef](#)]
18. Eamus, D.; Huete, A.; Yu, Q. Modelling Radiation Exchange and Energy Balances of Leaves and Canopies. *Veg. Dyn.* **2016**, *0*, 244–259. [[CrossRef](#)]
19. Chen, F.; Dudhia, J. Coupling and advanced land surface-hydrology model with the Penn State-NCAR MM5 modeling system. Part I: Model implementation and sensitivity. *Mon. Weather Rev.* **2001**, *129*, 569–585. [[CrossRef](#)]
20. Jarvis, P.G. Scaling processes and problems. *Plant. Cell Environ.* **1995**, *18*, 1079–1089. [[CrossRef](#)]
21. Lloyd, J.; Grace, J.; Miranda, A.C.; Meir, P.; Wong, S.C.; Miranda, H.S.; Wright, I.R.; Gash, J.H.C.; McIntyre, J. A simple calibrated model of Amazon rainforest productivity based on leaf biochemical properties. *Plant. Cell Environ.* **1995**, *18*, 1129–1145. [[CrossRef](#)]
22. Luo, X.; Chen, J.M.; Liu, J.; Black, T.A.; Croft, H.; Staebler, R.; He, L.; Arain, M.A.; Chen, B.; Mo, G.; et al. Comparison of Big-Leaf, Two-Big-Leaf, and Two-Leaf Upscaling Schemes for Evapotranspiration Estimation Using Coupled Carbon-Water Modeling. *J. Geophys. Res. Biogeosci.* **2018**, *123*, 207–225. [[CrossRef](#)]
23. Pleim, J.; Xiu, A. Development and testing of a surface flux and planetary boundary layer model for application in mesoscale models. *J. Appl. Meteorol.* **1995**, *34*, 16–32. [[CrossRef](#)]
24. De Pury, D.G.G.; Farquhar, G.D. Simple scaling of photosynthesis from leaves to canopies without the errors of big-leaf models. *Plant Cell Environ.* **1997**, *20*, 537–557. [[CrossRef](#)]
25. Wang, Y.; Leuning, R. A two-leaf model for canopy conductance, photosynthesis and partitioning of available energy I: Model description and comparison with a multi-layered model. *Agric. For. Meteorol.* **1998**, *91*, 89–111. [[CrossRef](#)]
26. Chen, N.; Wang, A.; An, J.; Zhang, Y.; Ji, R.; Jia, Q.; Zhao, Z.; Guan, D. Modeling Canopy Carbon and Water Fluxes Using a Multilayered Model over a Temperate Meadow in Inner Mongolia. *Int. J. Plant Prod.* **2020**, *14*, 141–154. [[CrossRef](#)]
27. Kobayashi, H.; Baldocchi, D.D.; Ryu, Y.; Chen, Q.; Ma, S.; Osuna, J.L.; Ustin, S.L. Modeling energy and carbon fluxes in a heterogeneous oak woodland: A three-dimensional approach. *Agric. For. Meteorol.* **2012**, *152*, 83–100. [[CrossRef](#)]
28. Liu, L.; Liu, X.; Chen, J.; Du, S.; Ma, Y.; Qian, X.; Chen, S.; Peng, D. Estimating maize GPP using near-infrared radiance of vegetation. *Sci. Remote Sens.* **2020**, *2*, 100009. [[CrossRef](#)]
29. Meyers, T.P.; Hollinger, S.E. An assessment of storage terms in the surface energy balance of maize and soybean. *Agric. For. Meteorol.* **2004**, *125*, 105–115. [[CrossRef](#)]
30. Campbell, G.S. Derivation of an angle density function for canopies with ellipsoidal leaf angle distributions. *Agric. For. Meteorol.* **1990**, *49*, 173–176. [[CrossRef](#)]
31. Campbell, G.S.; Norman, J.M. *An Introduction to Environmental Biophysics*, 2nd ed.; Springer-Verlag, Ed.; Springer: Pullman, WA, USA, 1998; Volume 6, ISBN 0387949372.
32. Bonan, G. Leaf Photosynthesis and Stomatal Conductance. In *Ecological Climatology*; Cambridge University Press: Cambridge, UK, 2015; pp. 241–263 ISBN 9781107339200.
33. Norman, J.M.; Welles, J.M.; McDermitt, D.K. Estimating canopy light-use and transpiration efficiencies from leaf measurements. *LICOR Appl. Note* **1991**, *105*, 19.
34. Medlyn, B.; Barrett, D.; Landsberg, J.; Sands, P.; Clement, R. Conversion of canopy intercepted radiation to photosynthate: Review of modelling approaches for regional scales. *Funct. Plant Biol.* **2003**, *30*, 153–169. [[CrossRef](#)] [[PubMed](#)]

35. Mercado, L.; Lloyd, J.; Carswell, F.; Malhi, Y.; Meir, P.; Nobre, A.D. Modelling Amazonian forest eddy covariance data: A comparison of big leaf versus sun/shade models for the C-14 tower at Manaus I. Canopy photosynthesis. *Acta Amaz.* **2006**, *36*, 69–82. [[CrossRef](#)]
36. Sprintsin, M.; Chen, J.M.; Desai, A.; Gough, C.M. Evaluation of leaf-to-canopy upscaling methodologies against carbon flux data in North America. *J. Geophys. Res. Biogeosci.* **2012**, *117*, 1–17. [[CrossRef](#)]
37. Jennings, S.A.; Koehler, A.K.; Nicklin, K.J.; Deva, C.; Sait, S.M.; Challinor, A.J. Global Potato Yields Increase Under Climate Change With Adaptation and CO₂ Fertilisation. *Front. Sustain. Food Syst.* **2020**, *4*, 519324. [[CrossRef](#)]
38. Quiroz, R.; Ramírez, D.A.; Kroschel, J.; Andrade-Piedra, J.; Barreda, C.; Condori, B.; Mares, V.; Monneveux, P.; Perez, W. Impact of climate change on the potato crop and biodiversity in its center of origin. *Open Agric.* **2018**, *3*, 273–283. [[CrossRef](#)]
39. Velez Betancourt, A.F. Estado del arte de la cadena de valor de la papa en Colombia. In *Cadenas Sostenibles Ante un Clima Cambiante. La Papa en Colombia*; Deutsche Gesellschaft für Internationale Zusammenarbeit (GIZ) GmbH Oficinas: Bogotá, Colombia, 2020; p. 102 ISBN 9789588945545.
40. Campos, H.; Ortiz, O. *The Potato Crop: Its Agricultural, Nutritional and Social Contribution to Humankind*; Springer Nature: Berlin, Germany, 2019; ISBN 9783030286835.
41. Mosquera Vásquez, T.; Del Castillo, S.; Gálvez, D.C.; Rodríguez, L.E. Breeding Differently: Participatory Selection and Scaling Up Innovations in Colombia. *Potato Res.* **2017**, *60*, 361–381. [[CrossRef](#)]
42. Soil Survey Staff. *Keys to Soil Taxonomy*, 12th ed.; USDA-Natural Resources Conservation Service: Washington, DC, USA, 2014; ISBN 0926487221.
43. Falge, E.; Baldocchi, D.; Olson, R.; Anthoni, P.; Aubinet, M.; Bernhofer, C.; Burba, G.; Ceulemans, R.; Clement, R.; Dolman, H.; et al. Gap filling strategies for defensible annual sums of net ecosystem exchange. *Agric. For. Meteorol.* **2001**, *107*, 43–69. [[CrossRef](#)]
44. Tagesson, T.; Fensholt, R.; Cropley, F.; Guiro, I.; Horion, S.; Ehammer, A.; Ardö, J. Dynamics in carbon exchange fluxes for a grazed semi-arid savanna ecosystem in West Africa. *Agric. Ecosyst. Environ.* **2015**, *205*, 15–24. [[CrossRef](#)]
45. Wang, Y.P.; Jarvis, P.G. Mean leaf angles for the ellipsoidal inclination angle distribution. *Agric. For. Meteorol.* **1988**, *43*, 319–321. [[CrossRef](#)]
46. Baly, E.C.C. The Kinetics of Photosynthesis. *Proc. R. Soc.* **1935**, *117*, 218–239. [[CrossRef](#)]
47. Smith, E.L. Photosynthesis in Relation to Light and Carbon Dioxide. *Proc. Natl. Acad. Sci. USA* **1936**, 504–511. [[CrossRef](#)] [[PubMed](#)]
48. Jassby, A.D.; Platt, T. Mathematical formulation of the relationship between photosynthesis and light for phytoplankton. *Limnol. Oceanogr.* **1976**, *21*, 540–547. [[CrossRef](#)]
49. Webb, W.L.; Newton, M.; Starr, D.; Url, S. Carbon Dioxide Exchange of *Alnus rubra*. A Mathematical Model. *Int. Assoc. Ecol.* **1974**, *17*, 281–291.
50. Lobo, F. de A.; de Barros, M.P.; Dalmagro, H.J.; Dalmolin, Â.C.; Pereira, W.E.; de Souza, É.C.; Vourlitis, G.L.; Rodríguez Ortiz, C.E. Fitting net photosynthetic light-response curves with Microsoft Excel - a critical look at the models. *Photosynthetica* **2013**, *51*, 445–456. [[CrossRef](#)]
51. Bonan, G. Mathematical Formulation of Biological Flux Rates. In *Climate Change and Terrestrial Ecosystem Modeling*; Cambridge University Press: Cambridge, UK, 2019; pp. 53–63 ISBN 9781107339217.
52. Sellers, P.J.; Berry, J.A.; Collatz, G.J.; Field, C.B.; Hall, F.G. Canopy reflectance, photosynthesis, and transpiration. III. A reanalysis using improved leaf models and a new canopy integration scheme. *Remote Sens. Environ.* **1992**, *42*, 187–216. [[CrossRef](#)]
53. Luo, Y.; Hui, D.; Cheng, W.; Coleman, J.S.; Johnson, D.W.; Sims, D.A. Canopy quantum yield in a mesocosm study. *Agric. For. Meteorol.* **2000**, *100*, 35–48. [[CrossRef](#)]
54. Singsaas, E.L.; Ort, D.R.; DeLucia, E.H. Variation in measured values of photosynthetic quantum yield in ecophysiological studies. *Oecologia* **2001**, *128*, 15–23. [[CrossRef](#)]
55. Park S, N. Achievable productivities of certain CAM plants: Basis for high values compared with C₃ and C₄ plants. *New Phytol.* **1991**, *119*, 183–205. [[CrossRef](#)]
56. Fang, L.; Zhang, S.; Zhang, G.; Liu, X.; Xia, X.; Zhang, S.; Xing, W.; Fang, X. Application of Five Light-Response Models in the Photosynthesis of *Populus × Euramericana* cv. ‘Zhonglin46’ Leaves. *Appl. Biochem. Biotechnol.* **2015**, *176*, 86–100. [[CrossRef](#)]
57. Ye, Z.P.; Duan, S.H.; Chen, X.M.; Duan, H.L.; Gao, C.P.; Kang, H.J.; An, T.; Zhou, S.X. Quantifying light response of photosynthesis: Addressing the long-standing limitations of non-rectangular hyperbolic model. *Photosynthetica* **2021**, *59*, 185–191. [[CrossRef](#)]
58. Ye, Z.; Zhao, Z. A modified rectangular hyperbola to describe the light-response curve of photosynthesis of *Bidens pilosa* L. grown under low and high light conditions. *Front. Agric. China* **2010**, *4*, 50–55. [[CrossRef](#)]
59. dos Santos Junior, U.M.; de Carvalho Gonçalves, J.F.; Fearnside, P.M. Measuring the impact of flooding on Amazonian trees: Photosynthetic response models for ten species flooded by hydroelectric dams. *Trees-Struct. Funct.* **2013**, *27*, 193–210. [[CrossRef](#)]
60. Aubinet, M.; Chermanne, B.; Vandenhaute, M.; Longdoz, B.; Yernaux, M.; Laitat, E. Long term carbon dioxide exchange above a mixed forest in the Belgian Ardennes. *Agric. For. Meteorol.* **2001**, *108*, 293–315. [[CrossRef](#)]
61. Moureaux, C.; Debacq, A.; Bodson, B.; Heinesch, B.; Aubinet, M. Annual net ecosystem carbon exchange by a sugar beet crop. *Agric. For. Meteorol.* **2006**, *139*, 25–39. [[CrossRef](#)]